The importance of spatial variability in the generation of secondary gravity waves from local body forces

Sharon L. Vadas and David C. Fritts

NorthWest Research Associates, CoRA division, Boulder, CO, USA

Received 30 May 2002; revised 1 August 2002; accepted 8 August 2002; published 26 October 2002.

[1] We hypothesized earlier that the zonal mean body force required to close the mesospheric jets is sporadic in time, and is composed of a large number of spatially and temporally localized body forces. To explore the effects of such localization, we randomly generate a series of localized, 3D body forces in the mesosphere which create a mean acceleration of $\sim$100 m s^{-1} day^{-1} over this forcing volume. Secondary waves are also generated, and because they have large vertical scales, phase speeds, and vertical group velocities, they may induce important variabilities in the lower thermosphere where they dissipate. We find that the secondary waves from spatially smoothed body forces have much smaller momentum fluxes, frequencies, and vertical group velocities. Thus, global models having coarse resolution may be missing a significant source of sporadic wave drag and its effect throughout the middle atmosphere and lower thermosphere. *INDEX TERMS:* 3384 Meteorology and Atmospheric Dynamics: Waves and tides; 3367 Meteorology and Atmospheric Dynamics: Theoretical modeling. **Citation:** Vadas, S. L., and D. C. Fritts, The importance of spatial variability in the generation of secondary gravity waves from local body forces, *Geophys. Res. Lett.*, *29*(20), 1984, doi:10.1029/2002GL015574, 2002.

1. Introduction

[2] Mean decelerations of the mean wind of $\sim$30–100 ms^{-1} day^{-1} have been inferred near the mesopause during summer and winter months in radar measurements and modeling studies [*Fritts and Vincent*, 1987; *Tsuda et al.*, 1990; *Holton*, 1983; *Roble and Ridley*, 1994; *Hamilton et al.*, 1995]. This drag force is sufficiently large to close the mesospheric jets and reverse the latitudinal gradient of temperature near the mesopause under solstice conditions. It is generally accepted that gravity wave breaking in the mesosphere applies this drag force. For dissipation depths of a scale height, this requires daily mean gravity wave momentum fluxes of $\sim$5–10 m^{2}s^{-2} [*Fritts and Yuan*, 1989; *Tsuda et al.*, 1990]. This force is generally parameterized in general circulation models (GCMs) and large-scale models as a slowly varying force with large spatial extents. However, the nature of the mesospheric wave breaking processes is likely highly variable spatially and temporally due to the localization of the tropospheric sources, the wave scales most important in momentum transport, and the nature of wave instability processes. For example, momentum fluxes as large as $\sim$60 m^{2}s^{-2} for hourly intervals have been measured by radar [*Fritts and Yuan*, 1989; *Reid et al.*, 1988], while estimates derived from airglow measurements [*Yamada et al.*, 2001] may be as large as $\sim$900 m^{2}s^{-2} locally [*Fritts et al.*, 2002]. Thus, mesospheric wave breaking clearly results in spatially and temporally-localized body forces.

[3] It is generally thought that a body force only creates an altered mean wind and residual circulation. However, *Vadas and Fritts* [2001] showed that secondary waves are also created if a body force is localized spatially and temporally. Our past work focused on the characteristics of secondary waves from single as well as multiple, equidistant, identical body forcings. Here, we generate a random distribution of spatially and temporally localized 3D, zonal body forces. These forces are directed zonally, and their magnitudes vary in x, y, and z. We also generate artificially-smoothed body forces to simulate how a GCM or large-scale model with large grid spacings would describe the gravity wave response.

2. Variable Body Forces

[4] We randomly generate 20, spatially- and temporally-localized, Gaussian, zonal body forces that occur within an hour and over a small volume of the mesosphere. The number of forces was chosen to yield a mean zonal acceleration of $\simeq$100 ms^{-1} day^{-1}. Unlike our previous work, the individual body forces here have differing diameters, depths, and force strengths. Each body force center is chosen randomly to lie within $x-x_0$ = [−300, 300] km, $y-y_0$ = [−300, 300] km, and $z-z_0$ = [−2.5, 2.5] km, where (x_0, y_0, z_0) is the central location of the 3D volume. The starting time of each force is chosen randomly within t = [0, 1] h. Each body force is introduced smoothly in time and is given by

$$D_F = (u_0/\sigma_t)[1 - \cos(2\pi t/\sigma_t)] \cdot \exp\left[-0.5\left(\frac{(x-\bar{x})^2}{\sigma_x^2} + \frac{(y-\bar{y})^2}{\sigma_y^2} + \frac{(z-\bar{z})^2}{\sigma_z^2}\right)\right] \quad (1)$$

for $t \leq \sigma_t$, and is zero for $t \geq \sigma_t$, where u_0 is the body force amplitude and (x, y, z) is the force center. We choose $\sigma_x = \sigma_y$. The full horizontal diameter $4.5\sigma_x$ is chosen randomly between 60 and 200 km along a boxcar probability distribution, (60 + 140α) km, where α is a random number between 0 and 1. The full depth, $\mathcal{D}_z = 4.5\sigma_z$ is chosen to lie between 10 and 30 km, but along a probability distribution that heavily emphasizes 10 km full depths over 30 km full depths: $\mathcal{D}_z = (10 + 20\alpha^p)$ km, p = 3. The time duration of each force, σ_t, is chosen to equal τ_c, where τ_c is the characteristic period formed by inserting the spatial scales

0094-8276/02/2002GL015574$05.00

of the body force into the dispersion relation. This is a reasonable choice, given that the temporal variability associated with the deposition of momentum is expected to be of order or greater than the primary wave period.

[5] The body force amplitude for each force is determined as follows. Suppose a primary wave has horizontal and vertical wavelengths λ_x and λ_z and horizontal and vertical wavenumbers $k = 2\pi/\lambda_x$ and $m = 2\pi/\lambda_z$, respectively. This wave's intrinsic phase speed is then $|c_0 - U| \simeq N\lambda_z/2\pi$ using the Boussinesq dispersion relation, where c_0 is its phase speed in the ground frame of reference and U is the background wind velocity. Assuming it breaks according to saturation theory, its horizontal velocity is constrained in amplitude to $u'_p \simeq |c_0 - U|$ [*Hodges*, 1967]. Using the Boussinesq continuity equation, $ku'_p + mw'_p = 0$, to determine the wave's vertical velocity (w'_p), the primary wave's time-averaged momentum flux per unit mass is

$$\overline{u'_p w'_p} \simeq N^2 \lambda_z^3 \lambda_x^{-1} / (8\pi^2). \quad (2)$$

[6] As is well known, the vertical divergence of the average momentum flux of the primary wave leads to the horizontal acceleration of the fluid:

$$D_F(\mathbf{x}, t) = -(1/\bar{\rho})\partial\left(\bar{\rho}\overline{u'_p w'_p}\right)/\partial z, \quad (3)$$

where $\bar{\rho} \propto \exp(-z/\mathrm{H})$ is the background density and H is the scale height. Assuming that equation (3) holds by averaging only over a single horizontal wavelength and that $\overline{u'_p w'_p}$ is approximately constant with height over the entire breaking region (under the saturation theory assumption), the resulting body force is

$$D_F \simeq \overline{u'_p w'_p}/\mathrm{H}. \quad (4)$$

If the primary wave deposits its momentum over the time interval $\sigma_t/2$, then the spatially-averaged body force amplitude created by this wave is $D_F\ \sigma_t/2$, and the body force amplitude is twice this average value, or

$$u_0 = \frac{N^2 \sigma_t \lambda_z^3}{8\pi^2 \lambda_x \mathrm{H}}. \quad (5)$$

[7] It is reasonable to assume that the full depth at half-maximum of the body force equals the primary wave vertical wavelength, $4.5\sigma_z/2 \simeq \lambda_z$, because wave breaking is often confined vertically by density stratification or shear. There is no similar confinement, however, in the horizontal. As an example, we set the full width at half-maximum of the body force equal to twice the primary wave's horizontal wavelength, $4.5\sigma_x/2 \simeq 2\lambda_x$, characteristic of a relatively compact wave packet. However, the primary wave packet may extend 5 or 10 times the horizontal wavelength of the primary wave. In addition, we choose $x_0 = y_0 = 0$, $z_0 = 90$ km, $N = 0.02\ \mathrm{s}^{-1}$, and $f = 0$. These secondary waves are not due to geostrophic adjustment. We employ the linear, Boussinesq model of *Vadas and Fritts* [2001] to determine the solution analytically, with 128, 128, and 256 grid points in x, y, and z, respectively. This model neglects the generation of secondary waves through nonlinear interactions. For the body force amplitudes used here, the secondary wave-wave interactions are unlikely to be important [*Vadas et al.*, 2002]. For the unsmoothed distribution, the grid point spacings are $dx = dy = 27$ km and $dz = 2.2$ km, while for the spatially smoothed distribution, $dx = dy = 107$ km and $dz = 2.2$ km. The zonal and meridional momentum flux (per unit mass) at (k, l, m) with spectral resolution dk, dl, and dm is $M_{uw} = \widetilde{u}_{\mathrm{GW}}\widetilde{w}^*_{\mathrm{GW}} dk dl dm/V$ and $M_{vw} = \widetilde{v}_{\mathrm{GW}}\ \widetilde{w}^*_{\mathrm{GW}} dk dl dm/V$ where $\widetilde{u}_{\mathrm{GW}}$, $\widetilde{v}_{\mathrm{GW}}$ and $\widetilde{w}_{\mathrm{GW}}$ are Fourier transforms of the secondary wave velocity perturbations, an asterisk denotes the complex conjugate, and V is the 3D volume that contains all of the body forcings. The total momentum flux is $\int\int\int \sqrt{M_{uw}^2 + M_{vw}^2}$.

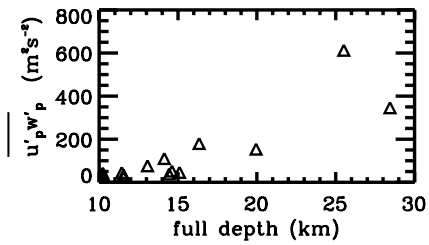

Figure 1. The primary wave momentum fluxes.

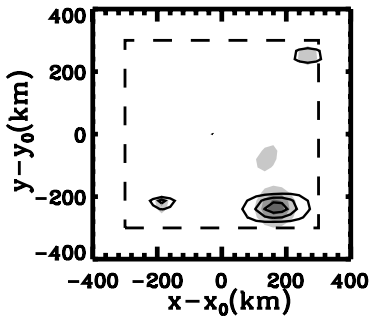

Figure 2. The integrated body forces (shading) in increments of 25% of the maximum value, which is 72 ms^{-1}. The mean zonal wind (solid contours) in intervals of 25% of the maximum value, which is 35 ms^{-1}. The dash box shows the region enclosing the force centers.

[8] In Figure 1, we show the primary wave momentum fluxes for the 20 body forces using equation (2). Only a few of the primary waves have large associated momentum fluxes. Figure 2 shows a horizontal slice of the body forces at $z = z_0$ integrated over the entire duration of the forcings, t = [0, 2.2] h. We also overlay the resulting mean zonal wind, which looks very similar to the integrated body forces and is highly localized spatially. Nearly all of the body forces occur within a depth of 14 km and a time span of an hour: $t \simeq$ [0.3–1.3] h or $\Delta t \simeq 1$ h. Averaging the zonal mean wind generated by these localized body forces over the volume $V = 600$ km $\times$ 600 km $\times$ 14 km, and multiplying by 24 hours, the mean zonal acceleration is $\simeq$100 $\mathrm{ms}^{-1}\ \mathrm{day}^{-1}$. Thus, this distribution of body forces yields a mean acceleration consistent with observations at the mesopause in summer and winter months.

[9] We integrate equation (4) over the volume and temporal duration of a force, and divide by the total volume and temporal duration for all of the forces. The average primary wave flux which leads to this body force is then

$$\overline{u'_p w'_p} \simeq (2\pi)^{3/2} \sigma_x \sigma_y \sigma_z u_0 \mathrm{H}/(V \Delta t), \quad (6)$$

using equation (1). We apply this formula separately for each body force and bin. The primary wave momentum flux spectrum is shown in Figure 3 where ω_i is the wave intrinsic frequency. It is sharply peaked at $\lambda_z \simeq 15$ km and $\omega_i \simeq N/3$. The total, average primary wave momentum flux which leads to these body forcings is $\overline{u_p' w_p'} = 8 \mathrm{m^2 s^{-2}}$.

[10] Because these body forces are temporally and spatially variable, upgoing and downgoing secondary gravity waves are created. (No secondary waves are created from a force with no temporal variability [*Vadas and Fritts*, 2001]). Here, 26% of the total energy of the forces goes into the generation of secondary waves. 25% of the secondary waves propagate upward and eastward (and northward and southward), while 25% propagate upward and westward (and northward and southward). Because our model is Boussinesq, the long-vertical-wavelength tail of the secondary wave spectrum has unrealistically large frequencies and phase speeds. To partly correct for this effect, we assume that the momentum fluxes calculated in our model are the same as in a compressible model. We estimate a wave's corrected intrinsic frequency by solving for the smaller root of the compressible dispersion relation:

$$\omega_i^4 - c_s^2\left(k_H^2 + m^2 + 1/4H^2\right)\omega_i^2 + c_s^2 k_H^2 N^2 = 0, \qquad (7)$$

where $c_s \simeq 300$ ms^{-1} is the sound speed and $k_H^2 = k^2 + l^2$ [*Gossard and Hooke*, 1975]. We note that the momentum fluxes for the larger vertical wavelength waves may differ. The corrected spectrum is not very different from the uncorrected spectrum because there is little momentum flux associated with waves having very large vertical wavelengths.

[11] In Figure 3, we overlay the secondary wave spectrum which depends on the spatial and temporal characteristics of the forces. The temporal variability used here yields a spectrum that is similar to that for impulsive body forcings, but with somewhat smaller wave frequencies,

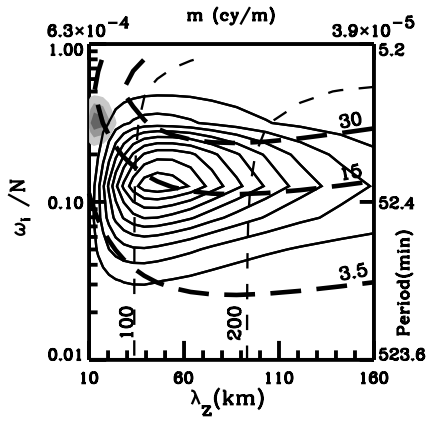

Figure 3. Vertical flux of zonal momentum in variance content form for the secondary waves in a quadrant (i.e., propagating upward and eastward, northward and southward) as light solid contours in increments of 0.005 m^2 s^{-2}. Light, short dashes indicate c_x when $l = 0$ in ms^{-1}. Thick, long dashes indicate c_{gz} in ms^{-1}. The shaded contours show the primary wave momentum flux spectrum in increments of 25% of the maximum value, which is 11 m^2 s^{-2}.

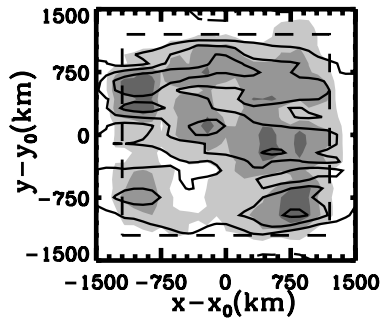

Figure 4. Same as in Figure 2, but for 320 spatially smoothed body forces. The maximum value of the integrated body forces is 11 ms^{-1}, while the maximum value of the zonal mean wind is 6 ms^{-1}.

vertical wavelengths and momentum fluxes [*Vadas et al*, 2002]. Overall, the total upgoing, radiated secondary wave momentum flux is 0.3 m^{2}s^{-2} at $z = z_0$. Thus, only 4% of the momentum flux of the primary waves is re-radiated as upgoing secondary waves. This is small, and would be insignificant if the secondary wave spectrum were identical to the primary wave spectrum. However, Figure 3 shows that the secondary wave spectrum is shifted significantly towards much larger vertical wavelengths than is the primary wave spectrum. (i.e., $\lambda_z \simeq 46$ km).

[12] We also overlay the horizontal phase speed, $c_x \equiv \omega_i/k$, in Figure. 3. Many of the secondary waves have much larger phase speeds than the primary breaking waves, and so can more easily penetrate into the thermosphere by escaping existing shears that would otherwise lead to dissipation near critical levels. We also overlay the vertical group velocity, $c_{gz} \equiv \partial\omega_i/\partial m$ in Figure 3. Significant portions of the secondary waves have vertical group velocities of 15–30 ms^{-1}. Waves with large vertical group velocities can propagate quickly into the lower thermosphere, and can dissipate (and deposit momentum) at higher altitudes than waves with smaller group velocities. Because the density decreases with height (and therefore the secondary wave momentum flux per unit mass increases with height), those secondary waves

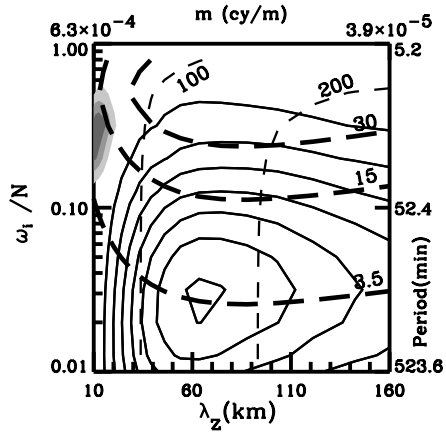

Figure 5. Same as in Figure 3, but for 320 spatially smoothed body forces. Light solid contours are in increments of 0.00025 m^{2}s^{-2}. The maximum value of the primary wave momentum flux spectrum is 9 m^{2}s^{-2}.

with large vertical group velocities, large horizontal phase speeds, and relatively large momentum fluxes may cause significant body forcing in the lower thermosphere where they dissipate sporadically in space and time.

3. Spatially Smoothed Body Forces

[13] In order to calculate the secondary wave spectrum from body forces which are smoothed by 550 km horizontally, we increase the length of the simulated region by 4 in both x and y. We also correspondingly generate $4 \times 4 \times 20 = 320$ random body forces to fill this larger area. Each force center is chosen randomly to lie within $x - x_0 = [-1200, 1200]$ km, $y - y_0 = [-1200, 1200]$ km, and $z - z_0 = [-2.5, 2.5]$ km. The resulting body force distribution is smoothed horizontally by a 5 degree boxcar window. The starting time and temporal duration of each force is as determined previously (prior to smoothing). Figure 4 shows a horizontal slice of the sum of all of the body forces integrated over the entire duration of the forcings, $t = [0, 2.2]$ h, along with the resulting mean zonal wind. As before, the mean zonal wind is strongest where the forces are strongest, although it is relatively spatially homogeneous as compared to Figure 2. Nearly all of the body forces occur within a 14 km depth and for a duration of an hour. Averaging the zonal mean wind generated by these body forcings over $V = 2400$ km $\times$ 2400 km $\times$ 14 km and multiplying by 24 hours, the average mean zonal acceleration here is $\simeq 110$ ms^{-1} day^{-1}. Although this average is a little high, this distribution of body forces approximately yields the observed mean acceleration at the mesopause in summer and winter months.

[14] Figure 5 shows the primary and secondary wave spectra. The total, average primary wave momentum flux which leads to these body forcings (prior to smoothing) is $\overline{u'_p w'_p} = 9 \mathrm{m^2 s^{-2}}$. The total upgoing, radiated secondary wave flux is 0.030 m^{2}s^{-2} at $z = z_0$, which is about 10 times smaller than that for the unsmoothed (body force) distribution. In addition, the secondary wave frequencies are much smaller, centering on approximately 2.8 hour periods rather than the 42 minute average period for the unsmoothed distribution. The vertical group velocities are much smaller also, and are centered on 3.5 ms^{-1} as compared to 15 ms^{-1} for the unsmoothed distribution. It is expected that this decrease in wave frequency and vertical group velocity will cause these waves to dissipate much lower in the thermosphere and therefore lead to even smaller responses in the lower thermosphere. We note that if these mesospheric body forces are smoothed zonally instead, the resulting secondary wave momentum fluxes are even smaller at mid and high latitudes, because the secondary waves generated in this case are a result of geostrophic adjustment which very inefficiently creates high-frequency secondary waves for these deep body forcings [*Vadas et al.*, 2002].

4. Discussion

[15] We have discussed a mechanism whereby secondary gravity waves are generated by a linear process; namely the deposition of momentum by primary breaking waves and the creation of spatially and temporally variable body forces. We found that many of these secondary waves have much larger vertical wavelengths, larger horizontal phase speeds, and larger vertical group velocities than the breaking primary waves. Because of this, many of these secondary waves may be able to escape the shears in the upper mesosphere and penetrate well into the lower thermosphere. Because the generation of these secondary waves is sporadic in space and time, the accelerations that are produced in the lower thermosphere where these waves dissipate will likely also be sporadic in space and time.

[16] In order to simulate how a large-scale model or GCM would describe such effects, we also investigated the effect of smoothing these body forces. We found that the momentum fluxes, vertical wavelengths, and frequencies of the resulting secondary waves decrease a substantial amount, thereby artificially reducing the effect these waves would have at greater altitudes.

[17] **Acknowledgments.** This research was supported by NASA under contract NAS5-02036 and by AFOSR under contract F49620-00-C-0008.

References

Fritts, D. C., and R. A. Vincent, Mesospheric momentum flux studies at Adelaide, Australia: Observations and a gravity wave/tidal interaction model, *J. Atmos. Sci.*, *44*, 605–619, 1987.

Fritts, D. C., and L. Yuan, Measurement of momentum fluxes near the summer mesopause at Poker Flat, Alaska, *J. Atmos. Sci.*, *46*, 2569–2579, 1989.

Fritts, D. C., S. L. Vadas, and Y. Yamada, An estimate of strong local body forcing and gravity wave radiation based on OH airglow and meteor radar observations, *Geophys. Res. Lett.*, *29*(10), 10.1029/2001GL013753, 2002.

Gossard, E. E., and W. H. Hooke, Waves in the Atmosphere, Elsevier Scientific Publishing Company, New York, pp. 112, 1975.

Hamilton, K., R. J. Wilson, J. D. Mahlman, and L. J. Umscheid, Climatology of the SKYHI troposphere-stratosphere-mesosphere general circulation model, *J. Atmos. Sci.*, *52*, 5–43, 1995.

Hodges, R. R. Jr., Generation of turbulence in the upper atmosphere by internal gravity waves, *J. Geophys. Res.*, *72*, 3455–3458, 1967.

Holton, J. R., The influence of gravity wave breaking on the general circulation of the middle atmosphere, *J. Atmos. Sci.*, *40*, 2497–2507, 1983.

Reid, I. M., R. Rüster, P. Czechowsky, and G. Schmidt, VHF radar measurements of momentum flux in the summer polar mesosphere over the Andenes (69°N, 16°E), Norway, *Geophys. Res. Lett.*, *15*, 1263–1266, 1988.

Roble, R. G., and E. C. Ridley, A thermosphere-ionosphere-mesosphere-electrodynamics general circulation model (TIME-GCM): equinox solar cycle minimum simulations (30–500km), *Geophys. Res. Lett.*, *21*, 417–420, 1994.

Tsuda, T., Y. Murayama, M. Yamamoto, S. Kato, and S. Fukao, Seasonal variation of momentum flux in the mesosphere observed with the MU radar, *Geophys. Res. Lett.*, *17*, 725–728, 1990.

Vadas, S. L., and D. C. Fritts, Gravity wave radiation and mean responses to local body forces in the atmosphere, *J. Atmos. Sci.*, *58*, 2249–2279, 2001.

Vadas, S. L., D. C. Fritts, and M. J. Alexander, "Mechanism for the generation of secondary waves in wave breaking regions", *JAS*, in press, 2002.

Yamada, Y., H. Fukunishi, T. Nakamura, and T. Tsuda, Breaking of small-scale gravity wave and transition to turbulence observed in OH airglow, *Geophys. Res. Lett.*, *28*, 2153–2156, 2001.

S. L. Vadas and D. C. Fritts, NWRA/CoRA Division, 3380 Mitchell Lane, Boulder, CO 80301, USA. (vasha@co-ra.com)